

Three-dimensional fast electron transport for ignition-scale inertial fusion capsules

J.J. Honrubia*

ETSI Industriales, Universidad Politécnica, Madrid, Spain

J. Meyer-ter-Vehn†

Max-Planck-Institut für Quantenoptik, Garching, Germany

(Dated: October 2, 2018)

Three-dimensional (3D) hybrid PIC simulations are presented to study electron energy transport and deposition in a full-scale fast ignition configuration. Multi-prong core heating close to ignition is found when a few GA, few PW beam is injected. Resistive beam filamentation in the corona seeds the 3D current pattern that penetrates the core. Ohmic heating is important in the low-density corona, while classical Coulomb deposition heats the core. Here highest energy densities (few Tbar at 10 keV) are observed at densities above 200 g/cm³. Energy coupling to the core ranges from 20 to 30%; it is enhanced by beam collimation and decreases when raising the beam particle energy from 1.5 to 5.5 MeV.

PACS numbers: 52.57.Kk, 52.65.Ww

Fast ignition of inertial fusion targets [1, 2] offers a promising alternative to the standard scheme of central hot spot ignition [3, 5]. Separating fuel compression from hot spot heating is expected to reduce compression and symmetry requirements significantly. Here we study Tabak's original proposal [1] to use a laser-driven electron beam to ignite the compressed core. Atzeni [4, 5] estimates that an energy of about 20 kJ is required to ignite 300 g/cm³ Deuterium-Tritium (DT) fuel when deposited in 20 ps on a 20 μm spot radius with 0.6 g/cm² stopping range. This implies a giga-ampere (GA), petawatt (PW) pulse of 1 MeV electrons. Little cones may be used to generate such beams and to guide them through the plasma corona [6, 8]. Recent experiments on cone guiding with 300 J, 0.5 PW laser pulses have demonstrated excellent (20 -30%) energy coupling from laser to core [6, 7]. For full-scale fast ignition, a 100 kJ, multi-PW beam is required including energy coupling. It will carry a few GA current, 10⁴ times larger than the Alfvén current that may limit transport due to magnetic self-interaction. Here the beam has to be transported over a distance of 100 - 200 μm between cone tip and core through a high-gradient plasma profile. This is the topic of the present paper.

In plasma, the beam current is compensated by return currents, which suppress the magnetic fields. But this beam is subject to filamentation instability. For collisionless plasma, linear growth rates have been studied in [9, 10], and particle-in-cell (PIC) simulation was used to trace the nonlinear evolution [11, 12]. This applies to low plasma densities, comparable to the beam density ($n_{beam}/n_{plasma} \geq 0.1$) but not to the high plasma densities considered in this paper. Full-scale PIC simulations are not yet feasible. They should include collisions and plasma resistivity to properly describe the return currents. Here we use a hybrid model adequate for describing self-magnetized transport in high-density

fuel. It treats only the relativistic beam electrons by PIC and models the background plasma by the return current density \mathbf{j}_r , tied to the electric field $\mathbf{E}=\eta\mathbf{j}_r$ by Ohm's law with resistivity η . Maxwell's equations are used in the form $\nabla\times\mathbf{B}=\mu_0\mathbf{j}$ and $\nabla\times\mathbf{E}=-\partial\mathbf{B}/\partial t$, where $\mathbf{j}=\mathbf{j}_b+\mathbf{j}_r$ is the sum of beam and return current density. The displacement current and charge separation effects can be neglected since in this high-density environment relaxation times and Debye lengths are much smaller than the sub-picosecond and micrometer scales of the resistive filamentation investigated here. The beam deposits energy into plasma electrons in two ways: by direct classical Coulomb deposition and via return current ohmic heating with power density ηj_r^2 . Electrons and ions are coupled by thermal energy transfer. A plasma density profile constant in time with equal electron and ion number densities is assumed. This model was proposed by Bell [13] and further developed by Davies [14] and Gremillet et al. [15]. First three-dimensional (3D) simulations based on this model were published in [15], showing 3D resistive filamentation. Gremillet et al. also derived the linear growth rates, now depending on resistivity η . The present version of the model is described in more detail in [16].

Recently, two-dimensional simulations of the cone-guided target experiment [6, 7] were published by Campbell et al. [17] and Mason [18]. Based on different hybrid codes, they could reproduce the measured core heating of 800 eV. Using the present model, we have obtained similar 2D results [19]; comparisons with the linear theory of the resistive filamentation instability are found in [20]. Here we present first three-dimensional simulations of electron transport and deposition in the high-density part of a fast ignition target. It is shown how 3D beam filamentation seeded in the corona leads to multi-hot-spot heating of the core close to DT ignition. The present study is motivated by the next generation of high-power

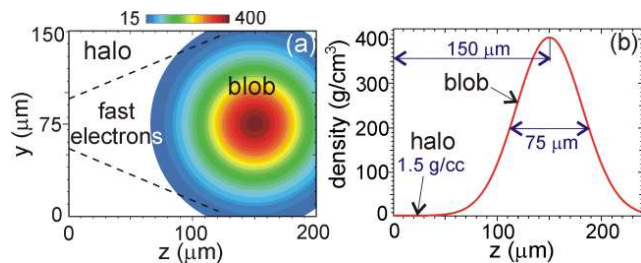


FIG. 1: Central cut through imploded target configuration: (a) isocontours of density in g/cm^3 , (b) density profile at $y=75 \mu\text{m}$.

facilities to demonstrate fast ignition [21, 22].

Simulation parameters. The simulated configuration is shown in figure 1. It consists of 0.2 mg DT fuel compressed into a spherical blob of $400 \text{ g}/\text{cm}^3$ peak density and $75 \mu\text{m}$ diameter (full width at half maximum, FWHM); it sits on a density pedestal of $1.5 \text{ g}/\text{cm}^3$ (the *halo*). A beam of fast electrons is injected from the left at $z = 0$. We imagine that it emerges from the tip of a cone at this position. The cone itself and the laser pulse generating the beam inside the cone are not simulated here. We rather model the injected beam in form of directed Gaussian electron distributions in radius and time with a spot radius of $20 \mu\text{m}$ and a duration of 10 ps, both at FWHM. The pulse has a power of 6 PW, a total energy of 60 kJ ($\approx 30 \text{ kJ}$ within FWHM) and is centered at 7 ps. The energy distribution of the beam electrons is assumed to be 1-D relativistic Maxwellian with temperatures depending on the local laser intensity I , also assumed Gaussian in radius and time, by the ponderomotive scaling formula $T_b \approx f \cdot m_e c^2 [(1 + I\lambda^2/13.7 \text{ GW})^{1/2} - 1]$, where λ is the wavelength. PIC simulations [23] give front factors $f \approx 1 - 3$, depending on the scale-length of the plasma in which the electrons are accelerated. For cone-guided fast ignition with 10 ps pulse durations and electron acceleration along the cone surface [24], the factor is expected to be larger than $f \approx 1$ which applies to sharp surfaces. Here we consider different cases with mean electron kinetic energies (averaged over the FWHM of the distributions in radius and time) in the range of $\langle E \rangle = 1.5 - 5.5 \text{ MeV}$; 2.5 MeV is taken as a reference value. This mean energy corresponds to a laser irradiance of $1.5 \times 10^{20} \text{ W}/\text{cm}^2$ (FWHM) at $0.35 \mu\text{m}$, assuming laser-to-electron transfer of 50% and beam compression by a factor of 3 due to geometrical cone convergence, in agreement with the results reported in [6, 7, 24, 25]. The initial angular distribution of fast electrons is obtained as in [26]. Electrons with energy $E = (\gamma - 1)m_e c^2$ are injected with a randomly chosen half-angle between 0 and $\tan^{-1}[h\sqrt{2}/(\gamma - 1)]$. The parameter h is used to adjust the initial beam opening half-angle as 22.5° (FWHM), consistent with the cone experiment [6, 7] and the simulations in [17, 18].

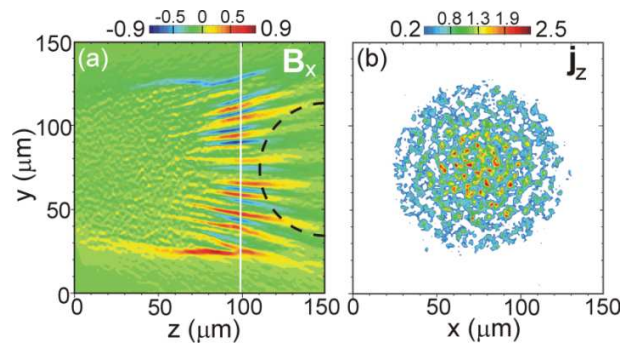


FIG. 2: (a) Central longitudinal cut of magnetic field B_x in kT generated by electrons with a mean kinetic energy of 2.5 MeV at the peak of the pulse, (b) perpendicular cut of beam current density j_z in units of $10^{14} \text{ A}/\text{cm}^2$ at $z=98 \mu\text{m}$. Plasma densities higher than $200 \text{ g}/\text{cm}^3$ are located inside the dashed circle.

The imploded fuel configuration shown in figure 1 has been scaled from that reported in [17, 18]. The main parameters of this configuration, the peak density of $400 \text{ g}/\text{cm}^3$, the distance of $150 \mu\text{m}$ from cone tip, and the initial plasma temperature, have been adapted from implosion simulations of cone targets with the code SARA-2D [27]. The plasma resistivity depends on the temperature distribution. The SARA-2D simulations indicate temperatures in the range of 300 eV to 1 keV. For simplicity, a uniform initial DT temperature of 500 eV is taken here, which sets the initial resistivity to a level of $10^{-8} \Omega\text{m}$. Concerning the numerical parameters, we have chosen a cell width of $1 \mu\text{m}$ in each coordinate, a time step of 3 fs, and a total number of 3.6×10^7 particles injected over the time interval of 0 - 14 ps. Free boundaries have been used in all simulations. Classical Spitzer resistivity is chosen for the DT plasma, and MPQeos tables [28] are used to compute electron and ion temperatures from the deposited energy.

Results. The injected current of 3.5 GA decays into filaments after a propagation distance of $z = 70 \mu\text{m}$; this is seen in figure 2(a) in terms of the B-field and in figure 2(b) in terms of current density. Actually we find that the filaments start to grow in the halo region ($z < 50 \mu\text{m}$) and are then strongly amplified in the density slopes of the blob. The growth rate is consistent with the linear theory developed in [15]. Resistive filamentation scales with plasma resistivity and therefore depends strongly on electron temperature T_e . In the lower density region, ohmic heating and Coulomb energy deposition lead to high electron temperatures with a mean value of $\langle T_e \rangle \approx 40 \text{ keV}$, much higher than the ion temperature T_i , and here magnetic fields saturate at levels of 100 T due to low resistivity. At higher densities ($z > 70 \mu\text{m}$), sufficient energy transfer from electrons to ions takes place, and we find $T_e \approx T_i \leq 20 \text{ keV}$. The corresponding ion temperature is plotted in figure 3(a). Here higher resistivity leads

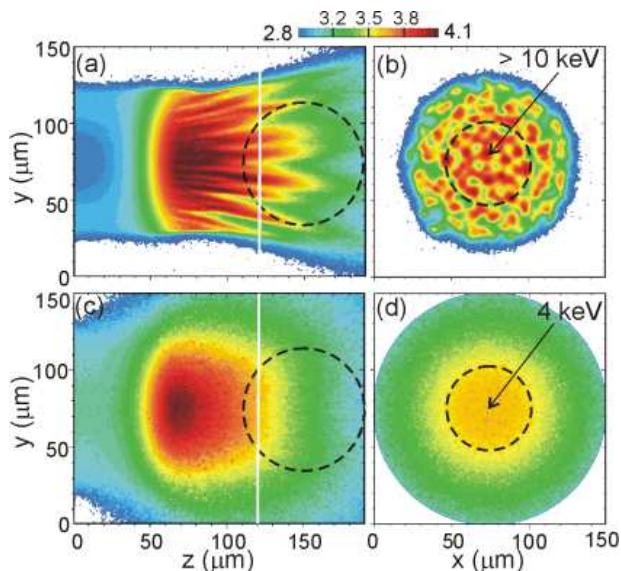


FIG. 3: Ion temperature of DT in units of $\log_{10}(T_i/\text{eV})$ at the end of the pulse of electrons with a mean kinetic energy of 2.5 MeV. (a) longitudinal cut at $x = 75 \mu\text{m}$, (b) transverse cut at $z = 120 \mu\text{m}$. Beam-generated fields have been artificially suppressed in (c) and (d). Plasma densities higher than 200 g/cm^3 are located inside the dashed circle.

to B -field of $\approx 1 \text{ kT}$ and enhanced filament growth. One should notice that the resistive filamentation observed here is weaker than that obtained from collisionless PIC simulations [11, 12] and has a wider spatial scale. Given the broad energy spectrum of beam electrons only those with lower energies ($< 1.5 \text{ MeV}$) are trapped in the current channels, while the others scatter freely and tend to smooth the structure. We find that both temperatures and B -fields are well described by the analytic scaling laws derived by Bell and Kingham [29]. We have also checked that filamentation persists for initial temperatures of 1 keV and halo densities up to 10 g/cm^3 , but disappears for beam kinetic energies $\langle E \rangle > 4.5 \text{ MeV}$.

The filaments shown in figure 2(b) carry about 10 MA beam current each. This beam current is almost completely compensated by the plasma return current, implying $j_r \approx -j_b$; the net current of a filament is only about 10 kA, consistent with the magnetic field strengths of 1 kT observed in figure 2(a). It is worthwhile emphasizing that the filamented current distribution heats electrons significantly more than a uniform current distribution of same total current because of the j_r^2 dependence of ohmic heating. This is how filamentation leads to enhanced beam stopping within the present model. It differs from the strong anomalous stopping found in PIC simulations [11, 12] for lower plasma densities (about $10 \times$ beam density). Sentoku et al. have interpreted this stopping as stochastic scattering of return current electrons by magnetic perturbations $|B|$ giving rise to an ad-

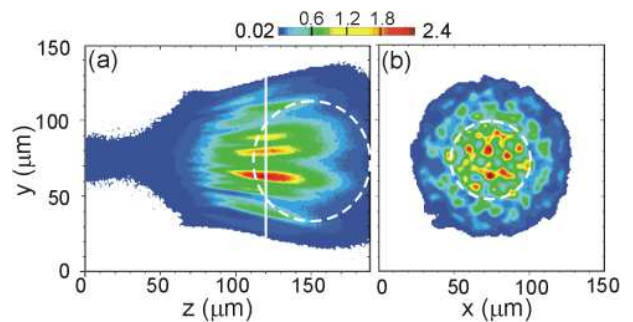


FIG. 4: Pressure of DT in Tbar for the electron pulse with a mean kinetic energy of 2.5 MeV: (a) longitudinal cut at $x = 75 \mu\text{m}$ and (b) transverse cut at $z = 120 \mu\text{m}$. Plasma densities higher than 200 g/cm^3 are located inside the dashed circle.

ditional effective resistivity $\eta_{eff} \approx |B|/(en_p)$. Even taking the scaling $|B| \propto n_p^{3/5}$ from [29], η_{eff} decreases with plasma density n_p . For the parameters of the present simulation, we find η_{eff} to be always smaller than the Spitzer resistivity. Therefore, we conclude that anomalous stopping of this kind plays no significant role here, in agreement with the results of Mason [18].

Figures 3 and 4 present the central results of this paper, showing DT fuel close to ignition. Notice that beam filamentation in the corona is responsible for the fragmented heating pattern in the core. Artificial suppression of the beam-generated fields (i.e. Coulomb deposition only) would lead to smooth core heating with a maximum temperature of 4 keV. This is shown in Figs. 3(c) and (d), for comparison. With fields present, a multi-hot-spot ignition region is formed in the high-density fuel with maximum temperatures beyond 10 keV. The conjecture here is that this will help ignition due to the nonlinear scaling of fusion reactivities with temperature. Actually, this needs to be confirmed in more detailed simulations, including hydrodynamics and fusion reaction physics in 3D geometry.

Here we give some estimates, based on the pressure distribution shown in figure 4. The DT ignition condition (see page 85 in [5]) can be written in compact form as $p_h R_h > 45(\rho_h/\rho_c)^{1/2} \text{ Tbar}\mu\text{m}$, where index h refers to hot fuel and index c to surrounding cold fuel. This condition combines the threshold values for $\rho_h R_h$ and T_h and holds for temperatures $5 < T_h/\text{keV} < 15$. From Figs. 3(a) and (b), we find for the central hot spot $2p_h R_h \approx 50 \text{ Tbar}\mu\text{m}$ in longitudinal direction. In transverse direction, it is $2p_h R_h \approx 15 \text{ Tbar}\mu\text{m}$, but here a number of neighboring hot spots will cooperate and $2p_c R_c \approx 50 \text{ Tbar}\mu\text{m}$, obtained from $p_c = 1 \text{ Tbar}$ and $2R_c = 50 \mu\text{m}$, may serve as an estimate. We conclude that the reference case shown in Figs. 3 and 4 is close to ignition. It should be understood that the core heating is almost exclusively due to Coulomb deposition of beam electrons.

Ohmic heating by return currents dominates in the halo, but plays only a minor role for the overall energy balance. Beam-generated fields turn out to contribute to the core heating indirectly, mediated by filamentation and collimation effects. Beam collimation is observed in figure 3(a) when compared with figure 3(c).

Figure 5 shows what fractions of the injected beam energy are deposited in different parts of the target. The total deposition, given versus beam kinetic energy $\langle E \rangle$, drops from 90% to 40%, when raising $\langle E \rangle$ from 1.5 to 5.5 MeV. Most of the deposition is due to classical Coulomb collisions, consistent with the areal density of 2.9 g/cm^2 along the axis. Notice that the other part of the energy is not deposited at all, but passes through the target and is lost. Clearly this makes average beam energies beyond 5 MeV prohibitive. The very important partition between deposition into high density core and low-density zones with $\rho < 200 \text{ g/cm}^3$ is also shown in figure 5. We find that the energy coupling to the core amounts to 30% at 1.5 MeV and 20% at 5 MeV. It is less sensitive to $\langle E \rangle$ than the coupling into the lower density regions. Of course, the core coupling strongly depends on the divergence angle of the injected beam, which is therefore a key parameter for fast ignition. In the present simulations, the core coupling efficiency degrades by 40%, when raising the angle from 22.5° to 30° . On the other hand, one should notice that magnetic pinching of the beam improves core coupling significantly. Suppressing all beam-generated fields in the simulations would lead to the dashed curves in figure 5.

Estimating the laser-to-fast-electron conversion efficiency to be 50%, we find a laser pulse energy of 100 - 150 kJ necessary to ignite a target. There may be possibilities to reduce this energy, e.g. by shortening the distance between cone tip and blob or by careful design of the cone to reduce beam divergence [30]. Certainly, transport in the cone needs to be included in more complete studies, in particular to account for the potential barrier [18] and filamentation [24] at the cone tip.

In conclusion, the message of this paper concerning fast ignition of inertial fusion targets is that a giga-ampere, multi-PW current can be transported through the steep gradients of the plasma corona toward the high-density fuel core. This is shown here for the first time in 3D geometry, using hybrid PIC simulation. Central questions could be answered: Collective magnetic effects play a major role for core heating, but in an indirect way. Resistive beam filamentation grows in the low-density halo and seeds the 3D multi-prong beam, which then penetrates the core. Of course, 3D simulation is crucial in this context.

In the core, collective behavior is suppressed due the large plasma-to-beam density ratio, and energy deposition takes place almost exclusively by classical Coulomb collisions. We find a fragmented hot spot configuration, and the fragmentation may actually help fuel ignition,

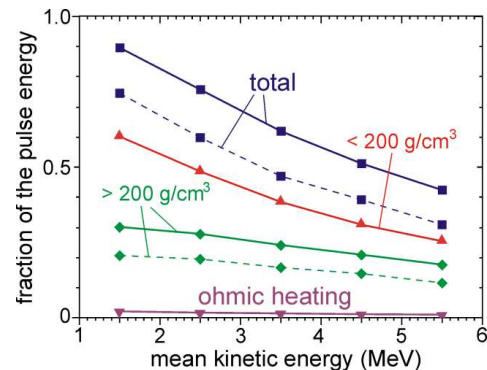


FIG. 5: Fraction of total pulse energy deposited in the target (squares), in low-density ($< 200 \text{ g/cm}^3$) zones (triangles) and in high-density ($> 200 \text{ g/cm}^3$) core (diamonds). Solid lines correspond to full simulations with beam-generated fields and Coulomb energy deposition. Dashed lines correspond to simulations with beam-generated fields suppressed. The fraction due to ohmic heating is small throughout.

since concentrating the energy in a number of prongs rather than heating the whole volume spanned by the prongs leads to higher temperatures and therefore to more heating by fusion products. The $\langle pR \rangle$ values obtained for the reference case indeed indicate that this case is close to ignition. More detailed simulations including hydrodynamics and fusion heating are now in progress to confirm this point.

Concerning collective beam deposition, we find, within the physical model used here, that indeed beam filamentation enhances ohmic heating, because it depends quadratically on the return current density j_r . But this additional deposition is not identical with the anomalous stopping found in PIC simulations at lower densities. It also contributes little to the overall energy balance in the present simulation of fast ignition. Rather the self-generated B-fields help by collimating the relativistic beam, and this improves the coupling efficiency substantially.

This work was supported by the research grant FTN2003-6901 of the Spanish Ministry of Education and by the Association EURATOM - IPP Garching in the framework of IFE Keep-in-Touch Activities and the Fusion Mobility Programme.

* Electronic address: javier.honrubia@upm.es

† Electronic address: juergen.meyer-ter-vehn@mpq.mpg.de

- [1] M. Tabak et al., Phys. Plasmas **1**, 1626 (1994).
- [2] M. Tabak et al., Phys. Plasmas **12**, 052708 (2005).
- [3] J. Lindl, Phys. Plasmas **11**, 339 (2004).
- [4] S. Atzeni, Phys. Plasmas **6**, 3316 (1999).
- [5] S. Atzeni and J. Meyer-ter-Vehn, *The Physics of Inertial Fusion*, Oxford Univ. Press, New York (2004).

- [6] R. Kodama et al., *Nature* **412**, 798 (2001)
- [7] R. Kodama et al., *Nature* **418**, 933 (2002).
- [8] R.B. Stephens et al., *Phys. Rev. Lett.* **91**, 185001 (2003).
- [9] L.O. Silva et al., *Phys. Plasmas* **9**, 2458 (2002).
- [10] A. Bret et al., *Phys. Rev. Lett.* **94**, 115002 (2005).
- [11] M. Honda, J. Meyer-ter-Vehn and A. Pukhov, *Phys. Rev. Lett.* **85**, 2128 (2000).
- [12] Y. Sentoku et al., *Phys. Rev. Lett.* **90**, 155001 (2003).
- [13] A.R. Bell et al., *Plasma Phys. Control. Fusion* **39**, 653 (1997)
- [14] J.R. Davies, *Phys. Rev. E* **65**, 026407 (2002).
- [15] L. Gremillet et al., *Phys. Plasmas* **9**, 941 (2002).
- [16] J.J. Honrubia, et al., *Phys. Plasmas* **12**, 052708 (2005).
- [17] R.B. Campbell et al., *Phys. Rev. Lett.* **94**, 055001 (2005).
- [18] R.J. Mason, *Phys. Rev. Lett.* **96**, 035001 (2006).
- [19] J.J. Honrubia and J. Meyer-ter-Vehn, *J. Phys. IV* **133**, 361 (2006).
- [20] J. Meyer-ter-Vehn et al., *Plasma Phys. and Control. Fusion* **47**, B807 (2005).
- [21] M. Dunne, *Nature Physics* **2**, 2 (2006).
- [22] K. Mima et al., *Fus. Sci. and Technol.* **49**, 358 (2006).
- [23] A. Pukhov, Zh-M. Sheng and J. Meyer-ter-Vehn, *Phys. Plasmas* **6**, 2847 (1999).
- [24] Y. Sentoku et al., *Phys. Plasmas* **11**, 3083 (2004).
- [25] R. Kodama et al., *Nucl. Fusion* **44**, S276 (2004).
- [26] J.J. Honrubia et al., *Laser Part. Beams* **24**, 217 (2006).
- [27] J.J. Honrubia, *J. Quant. Spectrosc. Radiat. Transf.* **49**, 491 (1993).
- [28] A.J. Kemp and J. Meyer-ter-Vehn, *Nucl. Instr. Methods in Phys. Res. A* **415**, 674 (1998).
- [29] A.R. Bell and R.J. Kingham, *Phys. Rev. Lett.* **91**, 035003 (2003).
- [30] R. Kodama et al., *Nature* **432**, 1005 (2004)